Journal of Colloid and Interface Science **249,** 8–21 (2002)
doi:10.1006/jcis.2002.8236, available online at http://www.idealibrary.com on IDEAL®

Th Uptake on Montmorillonite: A Powder and Polarized Extended X-Ray Absorption Fine Structure (EXAFS) Study

Rainer Dähn,*,[1] André M. Scheidegger,* Alain Manceau,† Enzo Curti,* Bart Baeyens,*
Michael H. Bradbury,* and Daniel Chateigner‡

*Waste Management Laboratory, Paul Scherrer Institut, Villigen, CH-5232, Switzerland; †Environmental Geochemistry Group, LGIT, University J. Fourier, BP 53, F-38041 Grenoble Cedex 9, France; and ‡Lab. Cristallographie et science des Matériaux, ISMRA, F-14050 Caen, France

Received October 10, 2001; accepted January 12, 2002

The uptake process of Th(IV) onto montmorillonite was studied using powder and polarized-EXAFS (P-EXAFS) spectroscopy. Sorption samples were prepared in 0.1 M $NaClO_4$ solutions either undersaturated (pH 2 and 3, $[Th]_{initial}$: 2.7×10^{-6} to 4×10^{-4} M) or supersatured (pH 5, $[Th]_{initial}$: 4.3×10^{-5} to 4×10^{-4} M) with respect to amorphous ThO_2. Th loading varied between 1–157 μmol/g at pH 3 and 14–166 μmol/g at pH 5 and equaled 41 μmol/g at pH 2. At pH 5 and high surface loading the EXAFS spectrum resembled that of amorphous $Th(OH)_4$, suggesting the precipitation of a Th hydrous hydroxide. At low and intermediate surface coverage two O coordination shells at ~2.24 and ~2.48 Å, and one Si shell at 3.81–3.88 Å, were systematically observed regardless of pH. The formation of Th nucleation products and Th–Si solution complexes and the sorption of Th on a silica precipitate were excluded from the EXAFS spectra analysis and solution chemistry. In these conditions, Th was shown to bond the montmorillonite surface by sharing double corners with Si tetrahedra. This structural interpretation is consistent with surface coverage calculations which showed that the edge sites were saturated in the two highest concentrated samples (34 and 157 μmol/g) at pH 3.

Key Words: **Th; montmorillonite; uptake; EXAFS; polarized EXAFS; surface complex.**

1. INTRODUCTION

Thorium is a naturally occurring, weakly radioactive element which is predominately (>99%) present as thorium-232 (half-life 1.41×10^{10} years). It occurs in a single redox state (+IV) and is therefore a suitable analogue for other tetravalent actinides. Thorium is used in a wide array of industrial products and processes (1). For example, Th acts as a catalyst for the oxidation of ammonia to nitric acid, and it is used in magnesium alloys and in tungsten filaments for light bulbs and electronic tubes. Thorium is also added during the manufacturing of refractive glass, allowing the production of smaller and more accurate camera lenses.

In natural systems, Th is an important trace element with accurately known source terms (2). It is widely distributed in small amounts in the Earth's crust, being about as abundant as lead or molybdenum and three times as abundant as uranium (1). Th is present in small amounts in rocks, soils, surface and ground waters, plants, and animals. For example, soils commonly contain an average of about 6 ppm thorium (1). There are several natural Th minerals, the most common being rare-earth thorium phosphate minerals (e.g., monazite) and thorium silicate minerals such as thorite and huttonite.

Large quantities of waste arising from mining and oil and gas extraction contain naturally occurring radioactive material such as uranium, thorium, and potassium (3). Furthermore, fly ashes from lignite power stations are contaminated with Th (4). Due to its radioactivity and widespread industrial application, Th has become an environmental contaminant. However, the most critical environmental aspect concerning Th is its safe disposal in nuclear waste repositories. The flow of ground water through a repository can potentially result in the release of radionuclides such as Th from waste matrices into the environment. The release of radionuclides can be considerably retarded due to interactions with clay minerals. For example, dioctahedral aluminous clays are foreseen as a backfill material in the Swiss concept for a high-level radioactive waste repository (5). Thus, a detailed understanding of the sorption mechanisms of Th with montmorillonite and the extension to other tetravalent actinides is of great importance for the safety assessment of nuclear waste repositories.

Montmorillonite is a clay mineral with substantial isomorphic substitution. Montmorillonite possesses a 2 : 1 layered structure consisting of one octahedral sheet and two tetrahedral sheets (6). Exchangeable cations between the 2 : 1 units balance the negative charges generated by isomorphic substitution within the montmorillonite structure (7). The uptake kinetics of cation exchange is fast and the cations such as Na^+ and Ca^{2+} form outer-sphere surface complexes, which are easily exchanged with solute ions by varying the cationic composition of the solution. In addition to cation exchange there is a pH-dependent uptake of metals on montmorillonite (7). In this sorption process sorbate ions bond to the smectite surface by sharing one or

[1] To whom correspondence should be addressed. E-mail: Rainer.Daehn@psi.ch.

0021-9797/02 $35.00

several ligands (generally oxygens) with sorbent cations as isolated complexes. With increasing pH or sorbate cation concentration, metal precipitation can occur. If the precipitate consists of chemical species derived from both the aqueous solution and dissolution of the mineral, it is referred to as a coprecipitate (8).

In the past, metal uptake on montmorillonite has been studied mainly using wet chemistry methods. For example the uptake of Cu, U, Cd, Ni, Zn, and Ca on montmorillonite was investigated in this way (9–15). Based on batch sorption data and the macroscopic surface properties of montmorillonite a "mechanistic" surface complexation model was developed in our laboratory for the uptake of Ni, Zn, and Eu (16, 17).

Recently, uptake experiments on montmorillonite have been complemented by spectroscopic investigations. For example, Chen and Hayes (18) investigated Co uptake on montmorillonite using extended X-ray absorption fine structure (EXAFS) and suggested the formation of a Co precipitate at elevated pH (pH >7; high ionic strength) and outer-sphere complexation at lower pH. The uptake of Sr on montmorillonite resulted in the formation of outer-sphere complexes, even up to pH 10 (18). Strawn and Sparks (19) have used EXAFS to distinguish between inner- and outer-sphere complexes of Pb(II) on montmorillonite. At pH >6.8 and high ionic strength the formation of inner-sphere Pb complexes was proposed, whereas outer-sphere complexes of Pb seem to prevail at lower pH and ionic strength. The uptake of U(VI) on montmorillonite was investigated by Sylwester *et al*. (20) using EXAFS. The EXAFS data suggested that the uptake of the uranyl ion onto montmorillonite at low pH occurs via ion exchange, leaving the uranyl structure intact. At near-neutral pH and in the presence of a competing cation, inner-sphere complexation predominates.

Manceau *et al*. (21, 22) have demonstrated that it is possible to gain further information upon the uptake processes of metal ions onto clay minerals by applying P-EXAFS to layered clay minerals. In P-EXAFS the contributions of cations from the tetrahedral sheets (Si in montmorillonite) are minimized by orienting the (*ab*) plane parallel to the electric field vector ε of the incident X-ray beam. Conversely, the contribution of cations from the octahedral sheet (Al and Mg in montmorillonite) is extinguished in the perpendicular orientation of ε. P-EXAFS has been successfully used to determine uptake processes of Co and Zn on hectorite, and Ni on montmorillonite (23–27). For example, Dähn *et al*. (26, 27) observed the neoformation of a Ni-phyllosilicate phase upon Ni uptake on montmorillonite (STx-1) at high ionic strength and at near-neutral pH (0.3 M $NaClO_4$, pH 8, 111 μmol/g Ni sorbed on montmorillonite) using P-EXAFS.

In this study, we have investigated the uptake process of Th onto montmorillonite using powder EXAFS at initial Th concentrations ($[Th]_{initial}$) both undersaturated (pH 2 and 3) and oversaturated (pH 5) with respect to amorphous ThO_2. In addition, P-EXAFS measurements with Th treated self-supporting clay films prepared at pH 2 and 3 were conducted to investigate whether the sorbed Th is orientated with respect to the octahedral sheets of montmorillonite.

2. MATERIAL AND METHODS

2.1. Montmorillonite Purification and Characterization

The STx-1 montmorillonite used in this study was purchased from the Source Clay Minerals Repository of the Clay Minerals Society. XRD analyses of the "as received" montmorillonite indicated the presence of minor quantities of calcite, quartz, and kaolinite (less than 1 wt%). This natural clay contains only ~0.9 wt% Fe_2O_3. The material was converted to the homoionic Na form by thoroughly washing three times with 1 M $NaClO_4$. The <0.5 μm size fraction was separated by successive washing with deionized water, combined with centrifugation (15). Soluble hydroxy-aluminum compounds were removed by an acid treatment at pH 3.5 for 1 h. The pH was subsequently readjusted to 7.

Amorphous iron was dissolved through a dithionate–citrate–bicarbonate treatment (28). The amount of extractable iron was determined to be approximately 30% of the total iron content by inductively coupled plasma optical emission spectroscopy (ICP-OES) and total digestion of the sample. Aliquots of clay suspensions were prepared in 0.1 M $NaClO_4$ concentrations using dialysis methods (15). The final conditioned montmorillonite suspension was stored at 4°C in the dark to minimize microbial growth.

The cation exchange capacity (CEC) was determined to be 1010 meq kg^{-1} by using the isotopic dilution method with ^{45}Ca (29). The external surface area of the conditioned STx-1 Ca-montmorillonite was measured by the N_2-BET technique to be 89 $m^2\ g^{-1}$. This value is in reasonable agreement with that determined by Van Olphen *et al*. (84 $m^2 g^{-1}$ (30)).

2.2. Sample Preparation for Powder- and Polarized-EXAFS (P-EXAFS)

EXAFS and P-EXAFS samples were prepared at reaction conditions undersaturated (pH 2 and 3) and oversaturated (pH 5) with respect to amorphous ThO_2. Powder EXAFS samples were prepared from the suspensions at pH 3 as follows: 50 ml of conditioned and purified montmorillonite suspension (pH 7, 0.1 M $NaClO_4$) were added to a 0.1 M $NaClO_4$ solution. The pH was adjusted to 3 with 0.1 M HNO_3. Th was then added from a 10^{-3} M $Th(NO_3)_4 \cdot 5H_2O$ stock solution (pH 3.0, 0.1 M $NaClO_4$) and the pH was readjusted to 3 and kept constant during the experiment. This procedure resulted in a 250 ml suspension at a solid to liquid ratio of 2.4 g/l for all samples. The initial Th concentrations varied from 2.7×10^{-6} to 4×10^{-4} M.

The Th sorption experiments were conducted in a glove box under N_2 atmosphere (CO_2 and $O_2 < 5$ ppm). After a reaction time of 7 days the suspensions were centrifuged and the wet pastes were filled into Plexiglas holders, sealed, and stored for up to 7 days in a refrigerator to keep them moist prior to the powder EXAFS measurements. The supernatant solutions were analyzed for Th, Al, and Si by ICP-OES. The silica concentration after 7 days of reaction time in our sorption system amounted

to 360 μM. The Si release rate in the Th/montmorillonite system was determined to be 5.8×10^{-14} mol m^{-2} s^{-1} (pH 3). The rate agrees well with the range of 6–7.2 $\times 10^{-14}$ mol m^{-2} s^{-1} measured by Heydemann (31) over a nine-month period for the dissolution of montmorillonite at pH 3 and suggests that the addition of Th did not influence the Si dissolution rate. The Al concentration in solution ($[Al]_{aq}$) varied from 26 to 47 μM and did not show any time dependency. Again, the Al concentration agrees well with the Al concentration observed by Heydemann (31) in a Th-free montmorillonite system ($[Al]_{aq}$ = 30–47 μM, pH3).

The initial Th concentrations (2.7×10^{-6} to 4×10^{-4} M) and the reaction pH of 3 were chosen to achieve a wide range of Th loadings in the Th/montmorillonite system (1–157 μmol/g; relative Th uptake >80% in all samples) while ensuring that the bulk solutions remained undersaturated with respect to amorphous ThO_2. The stability of the Th stock solution (1×10^{-3} M $Th(NO_3)_4 \cdot 5H_2O$, pH 3.0) used for this study was investigated and it was observed that the Th concentration did not change over a time period of up to one year. This finding is supported by a study of Rai *et al*. (32) which indicated that a Th concentration of $\sim 10^{-2}$ M is stable up to a reaction time of 21 days in a supersaturated system at pH 3 (0.1 M $NaClO_4$).

To estimate the degree of saturation with respect to the solubility of Th (hydr)oxides we calculated the saturation index (SI) with respect to amorphous and crystalline ThO_2 using $\log K^{\circ}_{sp} = -12$ and -1.8 respectively (33). SI is defined as the ratio of the ion activity product, IAP, to the solubility constant K_{sp}. For example, for ThO_2 this yields $SI = (Th)^{4+}/[(H^+)^4\ K^{\circ}_{sp}]$, where $(Th)^{4+}$ and (H^+) are the activities of Th^{4+} and H^+ in solution. The calculation revealed that our solutions at pH 3 are greatly undersaturated with respect to amorphous ThO_2 (SI < 0.0004), but supersaturated with respect to the crystalline form. However, the mentioned data of Rai *et al*. (32) as well as our stability test clearly show that crystalline ThO_2 does not precipitate from such diluted solutions. The formation of crystalline ThO_2 first requires the precipitation of the amorphous form, followed by aging for long times. Thus, one can assume that Th removal from solution is not due to Th(hydr)oxides formation in solution at any time during the experiments. To the best of our knowledge, the solubility products of Th-silicate phases (e.g., thorite, huttonite) are not known.

Th speciation calculations based on the thermodynamic data of Baes and Messmer (34) revealed for a total Th concentration of 10^{-4} M that the dominating species is the free aqua ion Th^{4+} (89%). The remaining part consists of hydrolysis products such as $ThOH^{3+}$, $Th(OH)_2^{2+}$, and $Th(OH)_3^+$ ($[Th] < 8 \times 10^{-6}$ M).

At pH 5 (powder EXAFS), pH 2 (powder and polarized EXAFS), and pH 3 (polarized EXAFS) the clay suspensions were prepared using the same experimental procedure as described above. In the experiments at pH 5 the initial Th concentration varied between 4×10^{-5} and 4×10^{-4} M. In this case, the solutions were oversaturated with respect to amorphous ThO_2 (33).

Two self-supporting films for polarized EXAFS were prepared from suspensions, one at pH 2 and initial Th concentration of 10^{-4} M (SI(am. ThO_2) < 10^{-8}) and another at pH 3 and initial Th concentration of 4×10^{-5} M(SI(am. ThO_2) < 0.0004). To prevent any significant clay dissolution, a reaction time of 6 h was chosen for the pH 2 experiment. In spite of the short reaction time the procedure resulted in the removal of 99% of the Th from solution. To prepare highly oriented self-supporting films for P-EXAFS measurements 40 ml of the clay suspensions were slowly filtrated using a 47 mm diameter filter (Millipore, 0.4 μm pore size). The filtration was performed in a closed vessel under a continuous flow of Ar. Excess of salt and aqueous Th in the wet films was removed by careful washing with a few milliliters of deionized water before drying. The dried clay films were cut into eight slices and stacked on sample holders in order to get samples thick enough for fluorescence measurements. Again, the supernatant solutions were analyzed for Th, Si, and Al using ICP-OES.

In addition to the sorption samples, two reference aqueous solutions were prepared at pH 2. The first solution contained 10 mM Th_{aq} (0.1 M $NaClO_4$). The second reference solution contained 5 mM Th_{aq} and 0.1 mM Si_{aq} (0.1 M $NaClO_4$).

2.3. Quantitative Texture Analysis

X-ray diffraction texture analysis measurements were performed in reflection mode using a Huber texture goniometer mounted on a classical X-ray source. A point-focus incident beam of 0.5 × 0.5 mm^2 and Cu$K\alpha$ radiation were used. One slice of each self-supporting film was mounted on a single-crystal silicon wafer. Pole figures were measured using a position sensitive curved detector (INEL CPS 120) having a $2\theta_{max} = 120^{\circ}$ (35). This configuration allows a rapid measurement (i.e., without Bragg angle scanning) of the whole diffraction pattern at each tilt angle (ρ) between the film and the diffraction planes. Since self-supporting films of fine-grained layer minerals have an axially symmetric (fiber) texture (i.e., random in-plane distribution of crystallite *a* and *b* axes) the complete film texture can be obtained by measuring the inclination of (001) crystallographic planes off the sample surface (21). This was achieved by selecting the (004) reflection and scanning the tilt angle from $\rho = 0$ to $\rho = 85^{\circ}$, in 5° steps, with an integration time of 2 h for each tilt angle position. The densities of the orientation distribution were calculated from the ρ-scan integrated intensities using direct normalization and taking a density of zero for $\rho > 80^{\circ}$ (for details see (21)). Distribution densities are expressed as "multiple of a random distribution" or "mrd" (36), a perfectly random sample exhibiting constant densities of 1 mrd.

2.4. EXAFS Data Collection and Reduction

L_{III}-edge EXAFS spectra of Th were recorded at the Rossendorf Beamline (ROBL) (37) at the European Synchrotron Radiation Facility (ESRF), Grenoble, France using a Si (111)

TABLE 1
X-Ray Diffraction Data and EXAFS Results for Reference Substances

Compound	Bond	Method	R [Å]	CN	σ^2 [Å^2]	Link[a]	Reference[c]
ThO_2	Th–O	XRD	2.42	8			1
	Th–Th	XRD	3.96	12			1
	Th–O	EXAFS	2.42	7.2	0.005		This work
	Th–Th	EXAFS	3.96	12.7	0.005		This work
Thorite (α-$ThSiO_4$)	Th–O	XRD	2.36	4		equat.	2
	Th–O	XRD	2.47	4		axial	2
	Th–O	EXAFS	2.41	7.7	0.0[b]		3
	Th–O	EXAFS	2.38	8.5	0.005		This work
	Th–Si	XRD	3.16	2		axial	2
	Th–Si	XRD	3.90	4		equat.	2
	Th–Si	EXAFS	3.89	2.9	0.005[b]		3
	Th–Si	EXAFS	3.92	3.9	0.005		This work
	Th–Th	XRD	3.90	4	0.005[b]		2
	Th–Th	EXAFS	3.90	5.7	0.002[b]		3
	Th–Th	EXAFS	3.90	5.3	0.005		This work
Huttonite (β-$ThSiO_4$)	Th–O	XRD	2.46	5		equat.	2
	Th–O	XRD	2.57	4		axial	2
	Th–O	EXAFS	2.35	5.4	0.008[b]	equat.	4
	Th–O	EXAFS	2.55	3.8	0.007[b]	axial	4
	Th–O	EXAFS	2.32	5.3	0.002	equat.	This work
	Th–O	EXAFS	2.50	7.7	0.005	axial	This work
Th(aq) 30 mM	Th–O	EXAFS	2.43	11	0.007		5
Th(aq) 50 mM	Th–O	EXAFS	2.44	11.2	0.007		5
Th(aq) 10 mM	Th–O	EXAFS	2.45	10.4	0.005		This work
Th(aq) 5 mM, 0.1 mM Si(aq)	Th–O	EXAFS	2.45	10.8	0.005		This work

[a] The terminology axial and equatorial linkage is discussed in the text.
[b] Using experimental phase and amplitude functions.
[c] 1, Wyckhoff (42); 2, Taylor and Ewing (40); 3, Östhols *et al*. (43); 4, Farges (44); 5, Moll *et al*. (41).

double crystal monochromator. Higher order harmonics were suppressed by using Pt coated mirrors. The monochromator position was calibrated by assigning the first inflection point of the K-absorption edge of metallic Y foil to 17038 eV. Powder-EXAFS spectra were recorded at 45° and P-EXAFS spectra were recorded with the electric field vector ε at 10°, 35°, 55°, and 80° with respect to the film plane. Several scans were averaged to improve the signal to noise ratio. All spectra were measured at room temperature in fluorescence mode using a 4-element Ge solid-state detector.

Data reduction was carried out by using the WinXAS 97 2.0 software package (38). The energy was converted to photoelectron wave vector units (Å^{-1}) by assigning the origin E_0 to the first inflection point of the absorption edge. Radial structure functions (RSFs) were obtained by Fourier transforming k^3-weighted $\chi(k)$ functions between 2.9 and 10 Å^{-1} using a Bessel window function with a smoothing parameter of 4. All fits were performed in R-space in the range from 0.7 to 4.0 Å. Amplitude and phase shift functions were calculated with FEFF 8.0 (39) using the structure of thorite (α-$ThSiO_4$ (40)) as a reference. The amplitude reduction factor (S_0^2) was set to 1.0 in order to reduce the number of free fit parameters (41).

The deviation between the fitted and the experimental spectra is given by the relative percentage of residual (%Res):

$$\%\mathrm{Res} = \frac{\sum_{i=1}^{N} |y_{\mathrm{exp}}(i) - y_{\mathrm{theo}}(i)|}{\sum_{i=1}^{N} y_{\mathrm{exp}}(i)} \cdot 100$$

with N the number of points in the fit window, and y_{exp} and y_{theo} the experimental and theoretical RSF values, respectively. Errors on structural parameters were estimated from the analysis of a series of reference compounds (see Table 1). The precision was estimated to be about ±0.02 Å for interatomic distances (R) and about ±25% for coordination numbers (CN).

3. RESULTS

3.1. Reference Compounds

Table 1 shows a comparison of structural parameters of reference compounds obtained by X-ray diffraction (XRD) with bond distances and coordination numbers obtained by EXAFS

data analysis. This comparison allows uncertainties to be estimated in the quantitative EXAFS analysis. The table also shows a comparison with previous Th EXAFS studies allowing the phase and amplitude functions used in this study to be tested. In most previous studies, EXAFS data analysis was performed using experimental phase and amplitude functions. In this study, however, theoretical phase and amplitude functions were calculated with FEFF 8.0 using the structure of thorite ($ThSiO_4$; (40)). The structure of thorite was chosen because it provides the appropriate scattering paths (Th–O, Th–Si, and Th–Th) for our data analysis.

The EXAFS analysis of crystalline ThO_2 yielded an average CN_{Th-O} of 7.2 ± 1.4 O atoms with $R_{Th-O} = 2.42$ Å ($\sigma^2 = 0.005$ Å^2) and $CN_{Th-Th} = 12.7 \pm 2.6$ with $R_{Th-Th} = 3.96$ Å ($\sigma^2 = 0.005$ Å^2). These structural parameters compare well with the structural parameters for ThO_2 as determined by XRD ($CN_{Th-O} = 8$, $R_{Th-O} = 2.42$ Å and $CN_{Th-Th} = 12$, $R_{Th-Th} = 3.96$ Å; (42)). Two other structural models were tested; thorite (α-$ThSiO_4$) and huttonite (β-$ThSiO_4$). In thorite the Th atom is coordinated by four axial and four equatorial O atoms. For the axial bonds each Th atom shares oxygens with the edges of 2 silica tetrahedra, with long Th–O and short Th–Si distances ($R_{Th-O} = 2.47$ Å, $R_{Th-Si} = 3.16$ Å; edge-sharing). Equatorial bonds link a Th atom with O atoms at the corner of silica tetrahedra, with short Th–O and long Th–Si distances ($R_{Th-O} = 2.36$ Å, $R_{Th-Si} = 3.90$ Å; corner-sharing). In huttonite, which has a more irregular structure (isomorphous to monazite) with nine O atoms coordinated with each Th atom, there is, instead, a range of Th–O distances, the shortest being 2.40 Å and the longest being 2.81 Å, but again the equatorial O atoms are on average closer to Th than the axial O atoms. The average distances measured by X-ray diffraction in this case are 2.46 and 2.57 Å (40). EXAFS data analysis of thorite resulted in average coordination numbers and bond distances of 8.5 ± 1.7 O atoms at 2.38 Å ($\sigma^2 = 0.005$ Å^2), of 3.9 ± 0.8 Si atoms at 3.92 Å ($\sigma^2 = 0.005$ Å^2) and of 5.3 ± 1.1 Th atoms at 3.90 Å ($\sigma^2 = 0.005$ Å^2). These structural parameters compare well with the results of a previous EXAFS study (7.7 O atoms at 2.41 Å ($\Delta\sigma^2 = 0.0$ Å^2), 2.9 Si atoms at 3.89 Å ($\sigma^2 = 0.005$ Å^2) and of 5.7 Th atoms at 3.90 Å ($\Delta\sigma^2 = 0.002$ Å^2), in which experimental phase and amplitude functions were used (43). Furthermore, the EXAFS structural parameters compare well with the XRD parameters for thorite, except that the 1st Si shell is not detected in EXAFS (four equatorial O at 2.36 Å, four axial O at 2.47 Å, two Si at 3.16 Å, four Si at 3.90 Å, and four Th at 3.90 Å, (40)). The EXAFS data analysis of huttonite resulted in shorter bond distances (2.32 and 2.50 Å) compared to XRD parameter (2.46 and 2.57 Å), whereas they agree well with distances (2.35 and 2.55 Å) obtained in an EXAFS study by Farges (44).

The EXAFS data analysis of a Th solution (10 mM Th in 0.01 M HNO_3, pH 3) resulted in ~10 neighboring O atoms at 2.45 Å (Table 1). This finding is in good agreement with a study by Moll *et al.* (41), in which ~11 Th–O pairs at 2.44 Å were determined for the spectrum of an acidic Th solution.

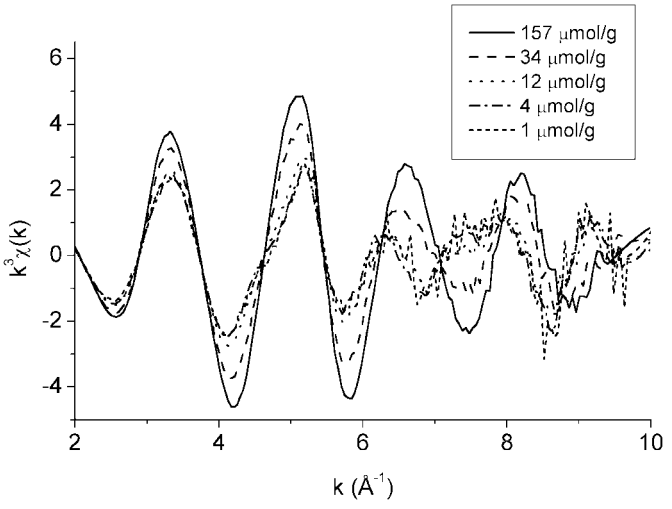

FIG. 1. k^3-weighted Th L_{III}-edge EXAFS spectra for Th sorbed on montmorillonite at pH 3 and various Th concentrations.

3.2. Powder EXAFS of Th-Sorbed Montmorillonite at pH 3

Figure 1 shows the k^3-weighted EXAFS spectra of montmorillonite treated with Th at pH 3 for 7 days. The Th loadings varied over a wide range from 1 to 157 μmol/g. The figure shows that the $k^3\chi(k)$ spectrum of the sample with the highest Th concentration (157 μmol/g) can be roughly approximated by a single sinusoidal oscillation over the entire k-range. With decreasing Th loading (34–1 μmol/g) the intensity of $k^3\chi(k)$ decreases and the wave frequency between ~6 and ~10 Å^{-1} increases. Furthermore, there is a clear asymmetry in the 4–8 Å^{-1} range which is most pronounced in the lower concentrated samples (1–12 μmol/g). These features indicate that the coordination of Th is changing with decreasing Th concentration.

The corresponding experimental RSFs are shown in Fig. 2. The figure shows that there are two RSF peaks for the highest

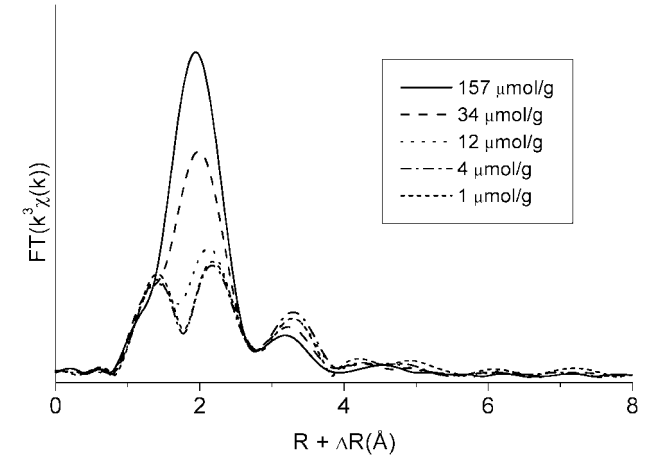

FIG. 2. RSFs of k^3-weighted Th L_{III}-edge EXAFS spectra for Th sorbed on montmorillonite at pH 3 and various Th concentrations.

TABLE 2
Structural Information Derived from the EXAFS Analysis of the Sorption Samples

	Th–O_1			Th–O_2			Th–Si				
Sample	CN_{Th-O1}	R_{Th-O1} [Å]	σ^{2a} [Å^2]	CN_{Th-O2}	R_{Th-O2} [Å]	σ^{2a} [Å^2]	CN_{Th-Si}	R_{Th-Si} [Å]	σ^{2a} [Å^2]	ΔE_0 [eV]	%Res
157 μmol/g, pH 3				8.1	2.44	0.005	2.1	3.87	0.005	8.2	12.9
34 μmol/g, pH 3				5.8	2.46	0.005	2.6	3.88	0.005	8.7	20.0
34 μmol/g, pH 3	2.9	2.23	0.002	8.6	2.45	0.005	2.5	3.84	0.005	4.9	9.9
12 μmol/g, pH 3	3.0	2.24	0.002	6.4	2.47	0.005	2.9	3.83	0.005	4.5	11.4
4 μmol/g, pH 3	3.0	2.24	0.002	5.8	2.48	0.005	2.9	3.83	0.005	4.4	13.0
1 μmol/g, pH 3	3.1	2.24	0.002	6.0	2.48	0.005	2.7	3.81	0.005	4.9	14.2
41 μmol/g, pH 2	3.1	2.22	0.002	7.8	2.46	0.005	2.8	3.81	0.005	3.8	16.2
166 μmol/g, pH 5	3.4	2.28	0.002	7.2	2.47	0.005	A reasonable fit could not be achieved			6.6	15.6
40 μmol/g, pH 5	3.0	2.26	0.002	7.4	2.45	0.005	1.4	3.87	0.005	5.4	9.1
14 μmol/g, pH 5	3.1	2.25	0.002	7.8	2.45	0.005	1.7	3.88	0.005	4.9	8.0

[a] Value held fixed during the fitting procedure.

concentrated samples (34–157 μmol/g) located at $R + \Delta R = 1.95$ Å and $R + \Delta R = 3.2$ Å. With decreasing Th loading, the first peak (Th–O contribution) decreases in amplitude and splits. In the lowest concentrated samples (1–4 μmol/g) there are RSF peaks located at $R + \Delta R = 1.4$ Å (short Th–O pair), at $R + \Delta R = 2.18$ Å (long Th–O pair) and at $R + \Delta R = 3.3$ Å. The intensity of the latter RSF peak increases with decreasing loading (157–1 μmol/g), and the figure suggests that the position of the peak slightly shifts to higher distances ($R + \Delta R = 3.2$–3.3 Å) as the Th loading decreases. Again, the RSFs indicate that the chemistry of Th changed with its concentration.

As mentioned in the experimental section (see Section 2.4) fitting was performed using a multishell approach (i.e., 0.7 to 4.0 Å range) in real space. The 1st coordination shell was fitted with Th–O pairs and the 2nd coordination shell was fitted with Th–Si pairs. As discussed later, we did not succeed in introducing Th–Th pairs in the EXAFS analysis of Th treated montmorillonite samples.

3.2.1. First RSF peak(s). As a first approach we tried to fit the Th–O coordination environment in the Th treated montmorillonite samples with a single O shell. With this fit strategy we previously succeeded in describing the Th–O coordination shell of Th in a 10 mM acidic aqueous solution (~11 O at 2.45 Å; Table 1, see Section 3.1). The fit approach with one oxygen shell yielded satisfactory results only for the sample with the highest Th loading (157 μmol/g, $CN_{Th-O2} = 8.1$ at 2.44 Å, Table 2). To reduce the number of fit parameters, the Debye–Waller factor (DW) of the oxygen shell was fixed to the value previously determined for the aqueous Th solution ($\sigma^2 = 0.005$ Å^2). We also tried to fit the sample with the second highest Th loading (34 μmol/g) with one O shell. The approach yielded a low Th–O coordination number ($CN_{Th-O} = 5.8$ at 2.46 Å) and a fit residual more than 50% larger than for the highest concentrated sample (Table 2). This finding is not surprising since Fig. 2 clearly indicates a splitting of the Th–O shell in two RSF peaks. The existence of two O shells is not uncommon in Th compounds and is found for example in thorite and huttonite (Table 1).

Consequently, in the next step the sorption samples loaded with 1–34 μmol/g Th were analyzed assuming two distinct Th–O pairs (Table 2). For crystal chemical reasons the total number of oxygen atoms in the first and second shell should not exceed 10–11 (41). Therefore the DW of the first oxygen shell was fixed to $\sigma^2 = 0.002$ Å^2 resulting in a total coordination number of ~10 for the two Th–O pairs. Table 2 shows that the first Th–O peak(s) of montmorillonite (1–34 μmol/g) treated with Th at pH 3 consists of ~3 Th–O pairs at 2.23–2.24 Å and ~6 to ~8 Th–O pairs at 2.45–2.48 Å. The corresponding experimental and simulated Fourier transforms (FTs) of a Th/montmorillonite sample (Th loading: 4 μmol/g) are illustrated in Fig. 3.

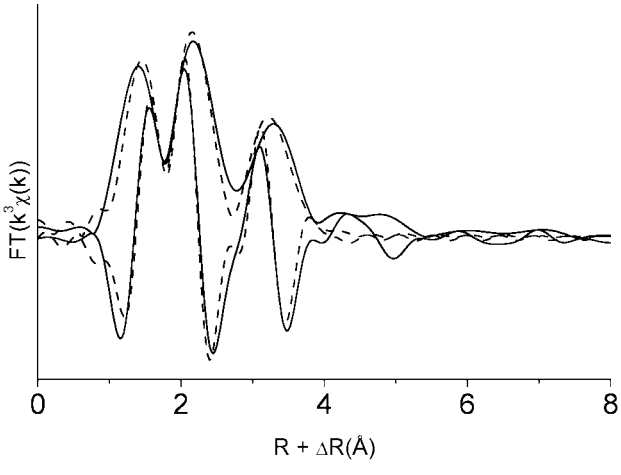

FIG. 3. Experimental and theoretical Fourier transforms (modulus and imaginary parts) of k^3-weighted Th L_{III}-edge EXAFS spectra for Th sorbed on montmorillonite (pH 3, 4 μmol/g Th). The simulations were performed by assuming Th–O_1, Th–O_2, and Th–Si pairs. The solid line represents the experimental data and the dashed line represents the fit of the real and imaginary parts.

We have used in our data analysis Gaussian radial distribution functions (harmonic model) to fit the experimental data. Östhols *et al*. (43) could also successfully fit their experimental data of the uptake of Th on amorphous silica using a harmonic approach. To check for the occurrence of non-Gaussian (anharmonic) distributions we used the cumulant expansion model (45) with the sample which contains 4 μmol/g Th. Also the fit with the cumulant expansion model was like all other fits performed in R space in the range from 0.7 to 4.0 Å. Since the second Th–O shell located at 2.45–2.48 Å is the dominant backscattering contribution in all spectra, the 3rd and 4th cumulant expansion was limited to this shell (46). The structural parameter significantly changed using the cumulant expansion. The Th–O distances of both O shells decreased by ∼0.07 Å. Furthermore, $CN_{Th–O1}$ decreased from 3 to 1.5, whereas $CN_{Th–O2}$ increased from 6 to 8. Only the Th–Si distances and the Si coordination number remained unaffected (for a detailed discussion see Section 3.2.2). Since a short distance of 2.17 Å has never been reported in Th compounds before, we suspect that the improvement of the fit is a purely mathematical artifact due to the introduction of two additional variable fit parameters (9 vs 7; number of independent parameter is 16 according to Nyquists theorem; (47)) and therefore we have disregarded this approach.

3.2.2. Second RSF peak. Figure 2 shows that in all spectra there is a RSF peak at $R + \Delta R \sim 3.2$–3.3 Å. Data analysis indicated that the peak is fitted best by assuming 2.1–2.9 Si atoms at a distance of 3.81–3.87 Å (Table 2). We also evaluated the possibility of the presence of a second Si shell. A second Si shell has been observed at 3.16 Å in a XRD study of thorite for example (40). Indeed, the approach indicated that a small number (<1) of Th–Si backscattering pairs located at 3.25–3.28 Å improved the fit residual by 20–40% compared to fits with two Th–O shells and one Th–Si shell. However, this alternative fit approach had only a minor influence on the structural parameters presented in Table 2 ($CN_{Th–Si}$ and $R_{Th–Si}$: ∼2.7 at 3.82–3.84 Å vs 2.7–2.9 at 3.81–3.83 Å). Any attempt to introduce Th–Th backscattering pairs in the fit failed. Further support for the absence of Th–Th pairs is given below.

3.3. Powder EXAFS of Th-Sorbed Montmorillonite at pH 2

In order to test the presence of a Th nucleation phase in the pH 3 samples, a Th montmorillonite sample was prepared under reaction condition (pH 2, [Th] = 41 μmol/g, 0.1 M $NaClO_4$), strongly undersaturated with respect to amorphous ThO_2 (see Section 2.2). Figure 4 shows the k^3-weighted Fourier back-transformed spectra of second RSF peaks ($R + \Delta R = 2.9$–3.7 Å; see Fig. 2 and dotted line in Fig. 7b) of montmorillonite samples treated with Th at pH 3 (1 μmol/g) and pH 2 (41 μmol/g). No difference in phase is detectable in these two spectra and the difference in amplitude is very small, suggesting that the second RSF peak in the two spectra has the same structural origin. Indeed, Table 2 confirms that the structural parameters obtained are similar in both samples (e.g., 2.7–2.8 Th–Si pairs at 3.81 Å). The similarity of the spectra furthermore prooves that no Th–Th pair is present in the pH 3 EXAFS samples.

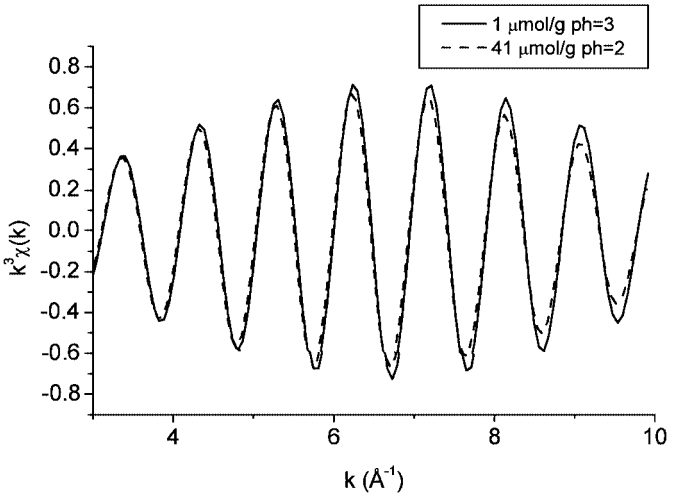

FIG. 4. k^3-weighted EXAFS functions obtained by Fourier back-transforming the second RSF peaks for a Th sorption sample at pH 3 and pH 2.

3.4. Polarized EXAFS of Th-Sorbed Montmorillonite at pH 2 and 3

Figure 5 shows the density of orientation of the c^* axes for the clay particles perpendicularly to the film prepared at pH 2. At $\rho = 0$ the density value is as high as 9.4 mrd, thus attesting that the dispersion of the individual crystallite c^* axes from perfect alignment is relatively low (21). The orientation distribution function was well reproduced by a Gaussian distribution (solid line in Fig. 5) having a full-width at half maximum (FWHM) of 43°. The sample approaches the distribution characteristic of a powder (i.e., 1 mrd) at $\rho \sim 40°$. The second film prepared at pH 3 (not shown) reached similar texture values as the film described above (9.8 mrd at $\rho = 0$ and a FWHM 43°).

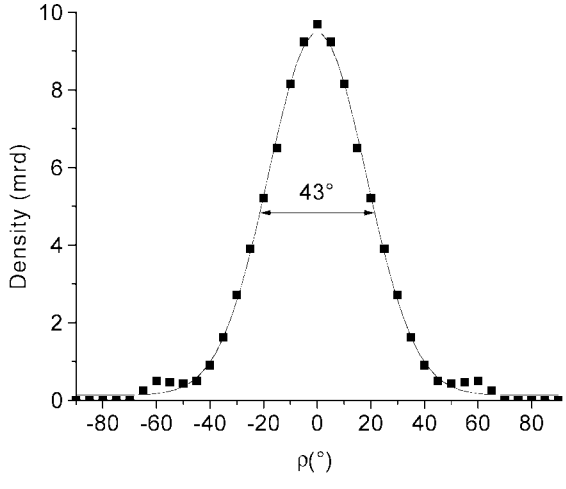

FIG. 5. Dispersion of c^* axes of montmorillonite particles off the film normal ($\rho = 0°$) for 41 μmol/g Th sorbed on montmorillonite at pH 2.

In a previous P-EXAFS study (27) texture values of a Ni treated self-supporting montmorillonite film (STx-1) were determined (13 mrd at $\rho = 0$ and a FWHM of 32.8°) which were sufficient to introduce pronounced anisotropy signatures in the P-EXAFS spectra. The angular dependence allowed identifying the presence of a neoformed Ni phyllosilicate phase in the sorption system. The texture values obtained in this study (∼10 mrd at $\rho = 0$, FWHM 43°) are slightly different than in the Ni study. Nevertheless if the Th sorption complexes are oriented relative to the film plane, their P-EXAFS spectra should display an angular dependence.

P-EXAFS spectra were recorded at $\alpha = 10°, 35°, 55°$, and 80° ($\alpha =$ the angle between the electric field vector and the plane of the self-supporting film). The k^3-weighted P-EXAFS spectra and the corresponding RSFs of the Th treated self-supporting clay film prepared at pH 2 are shown in Figs. 6a and 6b. The figures illustrate that the P-EXAFS spectra of the clay film have no significant polarization dependence. The same result was obtained for a self-supporting Th treated montmorillonite film (3 μmol/g; FWHM 43°, not shown) prepared at pH 3.

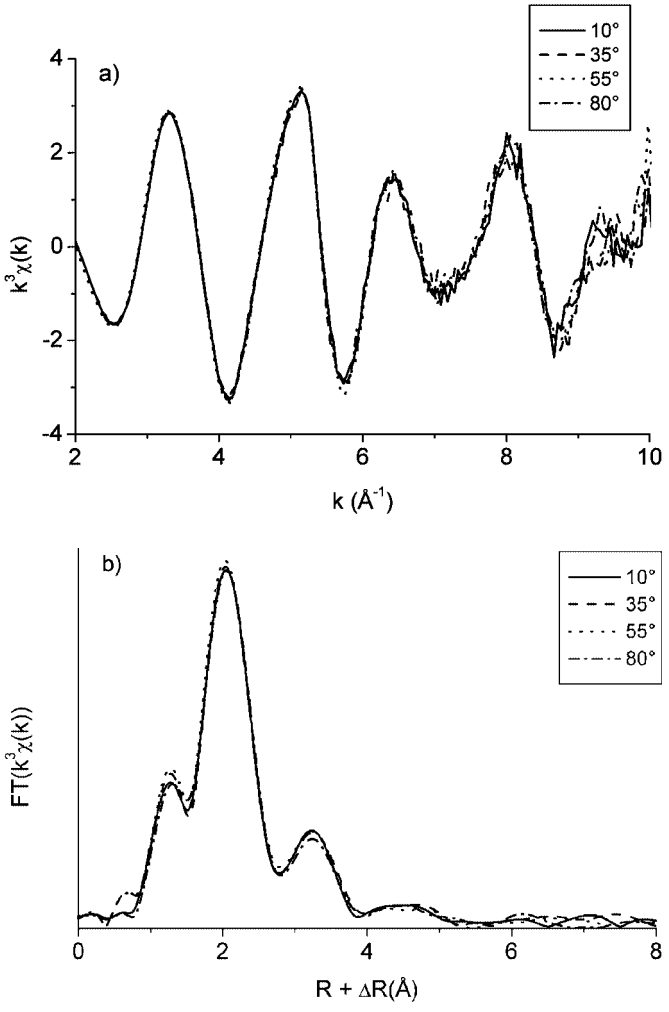

FIG. 6. (a) k^3-weighted Th L_{III}-edge polarized EXAFS spectra and (b) corresponding RSFs at experimental α angles of 10°, 35°, 55° and 80° for 41 μmol/g Th sorbed on montmorillonite at pH 2.

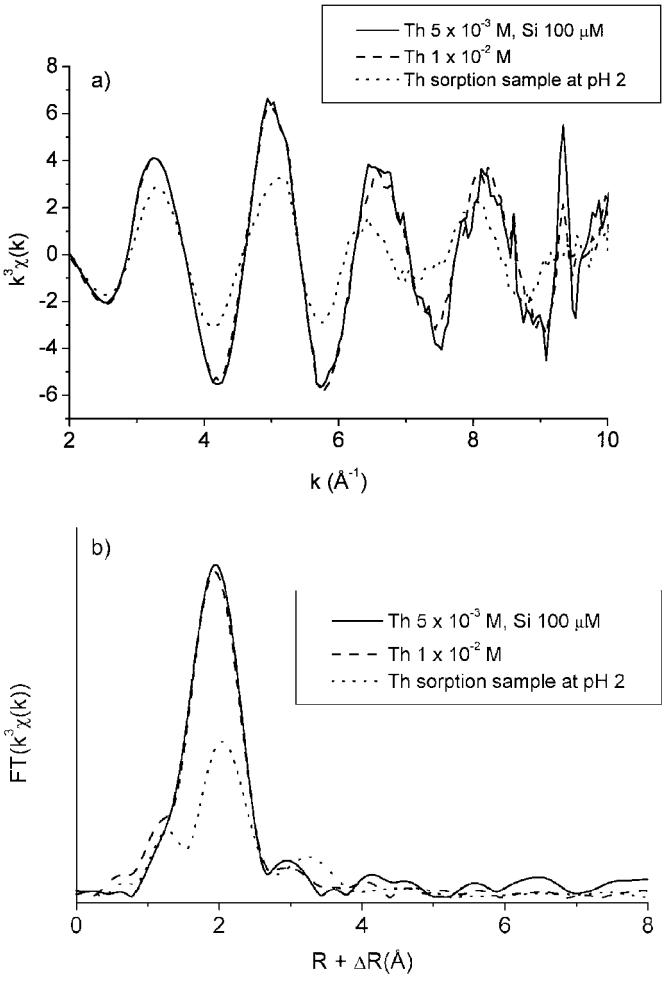

FIG. 7. (a) k^3-weighted Th L_{III}-edge EXAFS spectra and (b) RSFs for two Th aqueous solutions and a Th sorption sample at pH 2 (41 μmol/g).

3.5. Th Solutions

To investigate whether the Th–Si shell at 3.81–3.84 Å arises from Th adsorption on the clay or from a Th–Si solution complex, Th reference solutions with and without Si were prepared (pH 2; solution 1: $[Th]_{aq} = 10$ mM; solution 2: $[Th]_{aq} = 5$ mM, $[Si]_{aq} = 0.1$ mM; see Section 2.2). The Si concentration in the solution 2 was similar to that measured in the montmorillonite suspensions (0.16 mM, pH 2, reaction time: 6 h). Figure 7a shows the k^3-weighted EXAFS spectra of the Th reference solutions and a Th sorption sample (pH 2, 41 μmol/g). The k^3-weighted EXAFS spectrum of the Th sorption sample clearly differs from the spectra of the Th reference solutions, whereas the spectra of the reference solutions with and without Si are almost identical. This finding indicates that the sorption samples and the reference solution have a different structural origin. Further support for this finding is provided by the corresponding RSFs

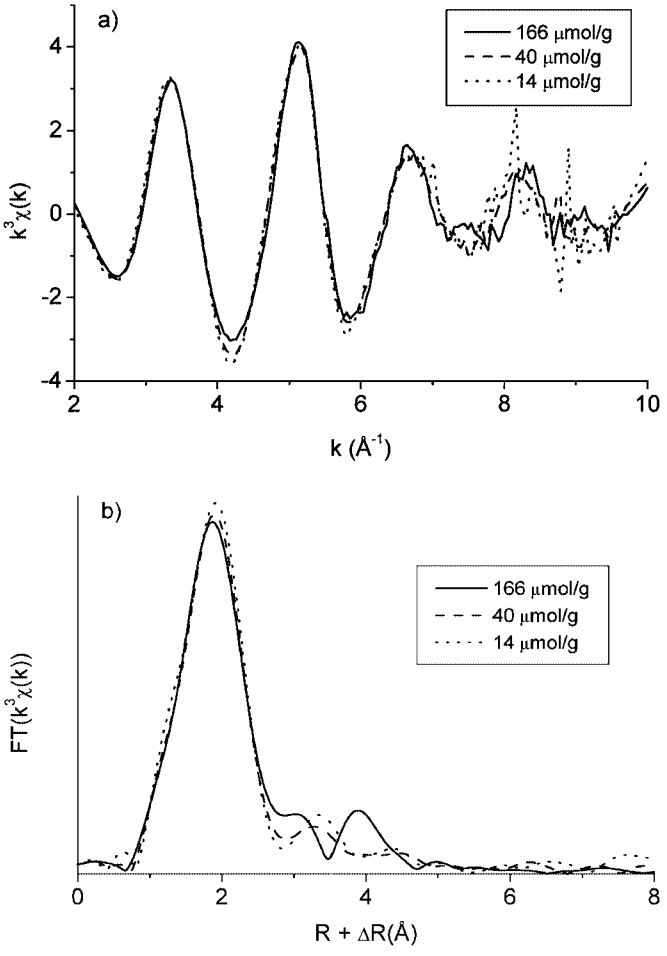

FIG. 8. (a) k^3-weighted Th L_{III}-edge EXAFS spectra and (b) corresponding RSFs for Th sorbed on montmorillonite at pH 5 and various Th concentrations.

in Fig. 7b. The figure indicates that the first RSF peak is not split in the reference solutions. Furthermore, the RSF peak at $R + \Delta R = 3.3$ Å, present in all the sorption samples at pH 2 and 3 (Fig. 2 and Fig. 6b), and which has been showed previously to be characteristic for Th–Si pairs (Table 2), is absent in the RSF spectra of the Th solutions and indicates that the Th–Si pair is due to the presence of the sorbent material and not to an aqueous Si complex. Finally, data analysis indicated that the aqueous samples could be fitted by assuming only one Th–O backscattering pair (Table 1). Accordingly, the first peak consists of 10–11 O atoms at 2.45 Å, which is in good agreement with a previous study on the structural environment of Th in an acidic solution (41).

3.6. Powder EXAFS of Th-Sorbed Montmorillonite at pH 5

To investigate whether Th nucleation occurs when the pH in the Th/montmorillonite system is raised, a set of sorption samples was prepared at pH 5 (Th loading: 14–166 μmol/g). As discussed in Section 2.2, the solutions from which these samples were made were oversaturated with respect to amorphous ThO_2.

Figure 8 shows k^3-weighted EXAFS spectra of montmorillonite treated with Th at pH 5 (Fig. 8a) and the corresponding RSFs (Fig. 8b). For the two samples with lower Th loadings (14 and 40 μmol/g) the amplitude and peak position of the first and the second RSF peaks ($R + \Delta R = 1.92$ and 3.28–3.34 Å) agree with those observed for higher Th loadings at pH 3 (Fig. 2). For the highest concentrated sample there is no second peak at $R + \Delta R = 3.3$ Å and instead a new RSF peak appears at a higher distance ($R + \Delta R = 3.88$ Å), suggesting a change in the average Th coordination environment.

The structural parameters of the pH 5 samples are listed in Table 2. Data analysis was conducted using the same fit constraints as those for the pH 3 samples (see Section 3.2). In all pH 5 samples the first RSF peak was described best by a short and a long Th–O backscattering pair (3.0–3.4 O at 2.25–2.28 Å and 7.2–7.8 O at 2.45–2.47 Å). These values compare well with the Th–O structural parameter at pH 3.

For the pH 5 samples with lower Th loading (14 and 40 μmol/g) data analysis further suggests a reduced number of Th–Si pairs compared to the sorption samples prepared at pH 3 (1.4–1.7 at ~3.87 Å vs 2.5–2.9 at ~3.83 Å; Table 2). The reduced $CN_{Th–Si}$ could be caused by the fact that a fraction of the Th atoms at pH 5 is no longer directly bonded to the montmorillonite surface and forms an outer-sphere complex. The reduced $CN_{Th–Si}$ can also be an indication of the presence of a small amount of Th–Th pairs. Th–Th and Th–Si pairs interfere destructively at 3.90 Å, and thus result in a reduced amplitude of the EXAFS spectra. For the pH 5 sample with the highest Th loading (166 μmol/g), neither a model with one Th–Th and one Th–Si pair nor a model with two Th–Th pairs at different distances provided a reasonable fit to the experimental spectrum. Nevertheless, it is possible to propose an "uptake" mode for Th in this sample. In Fig. 9 the EXAFS spectra of thorite (44) and amorphous $Th(OH)_4$ are compared to the 166 μmol/g Th sorption sample prepared at pH 5. The likeness of the sorption sample and the Th amorphous precipitate is striking and suggests

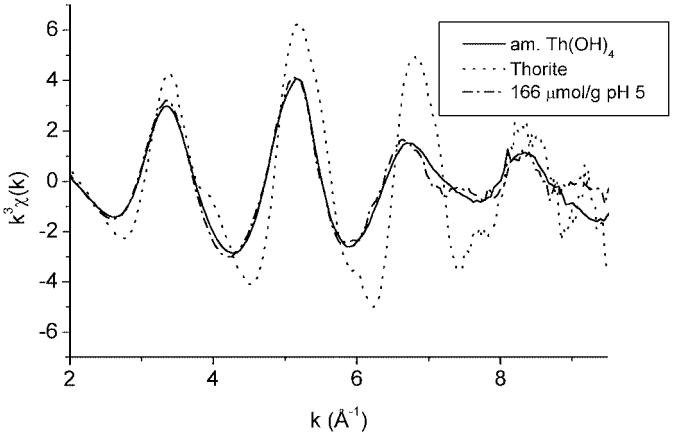

FIG. 9. Comparison of k^3-weighted EXAFS spectra for reference compounds and the highest concentrated Th sample.

the formation of a similar precipitate at high Th concentration. However, it was not possible to fit $Th(OH)_4$ data with just one or two Th–Th pairs.

4. DISCUSSION

4.1. Nature of the Sorbed Phase

EXAFS data of montmorillonite treated with Th at pH 2, 3, and 5 indicated the presence of a Th–Si pair at 3.81–3.88 Å in all Th sorbed montmorillonites, except for the most concentrated sample at pH 5. Furthermore, data analysis suggests the presence of two oxygen subshells in the first coordination environment of thorium (Table 2).

The finding of the presence of two oxygen subshells in the first coordination environment of thorium agrees with previous EXAFS studies on the uptake of cations onto montmorillonite (19, 20). Sylwester *et al*. (20) observed that at pH > 6.4 (0.1 M $NaClO_4$) the equatorial U–O pair splits when uranyl is sorbed onto montmorillonite. At lower pH (<0.01 M $NaClO_4$), however, no splitting was observed and the EXAFS structural parameters were similar to those of the aqueous uranyl ion. Similarly, Strawn and Sparks (19) observed that Pb uptake on montmorillonite resulted in a splitting of the oxygen shell at pH > 6.7 and 0.1 M $NaClO_4$ ionic strength, whereas the Pb–O distances and O coordination numbers were characteristic of Pb^{2+}(aq) at lower pH and ionic strength.

In the following we want to discuss whether the EXAFS findings can be explained by the formation of Th solution complexes, the precipitation of Th phases, or the sorption of Th onto the mineral substrate.

4.1.1. Complexation in solution. To evaluate whether the formation of Th solution complexes is an important process in our experimental system, EXAFS spectra of Si-free and Si-containing Th reference solutions were compared with the spectra of Th treated montmorillonite. While the spectra of the Si-free and Si-bearing solutions were identical, they showed no similarities with the spectra of Th treated montmorillonite, indicating that Th–Si solution complexes were not formed to any significant amount and are not relevant in this study (see Section 3.5, Fig. 7).

This finding is further supported by EXAFS data analysis. While the Th/montmorillonite samples exhibit two Th–O pairs and a Th–Si pair (Table 2), Th reference solutions were fit best with a single Th–O pair (Table 1). Th–O distances between 2.44 and 2.48 Å observed in the references solutions as well as the Th/montmorillonite samples are characteristic of Th–H_2O bonds (2.44–2.48 Å; Table 1 and (41, 48)).

4.1.2. Precipitation of a Th (hydr)oxide. This study indicated that, based on EXAFS data analysis, the presence of Th nucleation products can be excluded in montmorillonite samples which were treated with Th at lower pHs (pH 2 and 3; Fig. 4, Table 2, Sections 3.2 and 3.3).

In order to determine whether Th nucleation products were formed at higher pH values, uptake experiments were performed at pH 5 and initial Th concentrations exceeding the solubility limit of amorphous ThO_2 (pH 5; see Sections 2.2 and 3.6). The spectrum of the most concentrated Th/montmorillonite samples (166 μmol/g) is similar to the spectrum of amorphous $Th(OH)_4$ (Fig. 9), suggesting the formation of a Th-hydroxide-like precipitate in the sample. We were unable to fit the spectra with Th–Th pairs (see Table 2; Section 3.6). Östhols *et al*. (43) explained the absence of Th–Th pairs in amorphous $Th(OH)_4$ by proposing a large degree of disorder such that the spread in Th–Th distances prevents the detection of nearest Th neighbors.

In the lower concentrated samples prepared at pH 5 no similarity to the spectrum of amorphous $Th(OH)_4$ could be observed although also these samples were oversaturated with respect to amorphous ThO_2 (see Sections 2.2 and 3.6). We can only speculate that the likely absence of amorphous $Th(OH)_4$ is caused by a fast uptake of Th on montmorillonite resulting in remaining $[Th]_{aq} = 4 \times 10^{-6}$ M in solution which is undersaturated with respect to amorphous ThO_2 (SI = 0.004).

4.1.3. Th sorption on silica and dissolution of montmorillonite. The structural parameters obtained in our study (Table 2) agree with the findings of a previous EXAFS study on the uptake of Th on highly reactive amorphous silica at pH 3 ((43); 1.7–2.7 O at 2.27–2.34 Å vs 3.0–3.1 O at 2.24 Å (this study), 4.4–5.4 O at 2.53–2.56 Å vs 5.8–6.4 O at 2.47–2.48 Å (this study), and 1.3–2.7 Si at 3.79–3.89 Å vs 2.7–2.9 Si at 3.81–3.83 Å (this study)). Thus the sorption of Th on a silica phase is compatible with the EXAFS results and needs to be examined further.

XRD data indicated the presence of a small amount of quartz (<1%; see Section 2.1) in the conditioned clay material used in this study. Thus, quartz represents a potential SiO_2 sorbent in our system. The BET surface area of quartz (1 m^2/g; (49)) is however small compared to the BET surface area of montmorillonite (89 m^2/g; this study) and the amorphous silica used by Östhols *et al*. (170 m^2/g), making the sorption of Th on quartz an unlikely uptake process for Th in our experiments.

Another potential SiO_2 sorbent in our system is the presence of an amorphous silica phase that could have been formed by precipitation of Si from solution. The Si concentration in Th treated montmorillonite samples was monitored. The Si release rate ($\sim 10^{-14}$ mol m^{-2} s^{-1}) agrees well with the Si release rate of montmorillonite reported in the literature (see Section 2.2). The fact that the Si release rate was not modified due to the presence of Th indicates that the precipitation of Th-silicate is not likely. Since the solubility of amorphous Si is significantly higher (4100 μM; (50)) than in Th sorption experiments, we doubt that SiO_2 precipitates under the reaction conditions used, and therefore we conclude that sorption of Th onto an amorphous silica phase is not an important uptake process in this study. Besides Si, the concentration of Al in solution was monitored during the experiments. The low Al concentration (30–47 μM) indicated no change with time. The fact that $[Al]_{aq}$ remained constant while $[Si]_{aq}$ increased during the experiment might suggest the selective dissolution of tetrahedral SiO_4 layers

(incongruent dissolution), while octahedral Al-layer would remain stable.

Based on the previous discussion we can exclude the formation of a Th–Si solution complex, a Th precipitate (in all but the most concentrated sample at pH 5), and the uptake of Th on a SiO_2 phase. Thus, the only remaining possibility to explain the EXAFS data is a structural link of Th to the montmorillonite surface.

4.2. Topological Relationship between Th Polyhedra and Si Tetrahedra

The Th–Si bond length in all Th sorbed montmorillonites samples (3.81–3.88 Å; except the most concentrated sample at pH 5), is similar to the Th–Si EXAFS distance in thorite (3.90 Å) in which the bridging of Th to Si tetrahedra via corner-sharing linkage results in the presence of a short Th–O distance ($R_{Th–O} = 2.36$ Å, see Section 3.1). Therefore, by comparison with the thorite structure, we propose that Th bonds to the montmorillonite surface by sharing corners with tetrahedral Si and the short Th–O distance (2.23–2.24 Å) is assigned to the Si–O–Th bond (Fig. 10). The similarity of $CN_{Th–Si}$ (2.5–2.9) and $CN_{Th–O1}$ (∼3) values (Table 2) suggests that SiO_4 tetrahedra are linked to Th through a single O atom and that Th forms multidentate corner-sharing surface complexes. The data suggest the formation of a tridentate corner-sharing complex, but this can be questioned for the following reasons. The uncertainty on the coordination number in this EXAFS study is at least 25% (see Section 2.4). Thus, it is not possible to definitely differentiate between a double-, triple-, or fourfold-corner-sharing surface complex. Furthermore, one should keep in mind that EXAFS measures an averaged signal and thus an average coordination number is obtained. For example, a coordination number of three for Th–Si pairs could be explained not only by three neighboring Si "atoms," but also by a 1 : 1 mixture of two and four Si neighbors. As an example for possible coordination environments of Th in the Th/montmorillonite system, Fig. 10 illustrates how Th and Si could be connected via a double corner-sharing complex. In the figure, Th is coordinated to 6 O atoms from water molecules. Data analysis indicated 6–8 Th–O pairs at 2.44–2.48 Å in the Th-treated montmorillonite samples (Table 2) which attributed to Th–H_2O bonds (see Section 4.1). Since the total number of coordinated O atoms in solid Th compounds and aqueous solutions ranges from 8 to 11, a $CN_{Th–O2}$ of 6–8 is not unreasonable, assuming that two O atoms are coordinated to silica tetrahedral via a double corner-sharing complex.

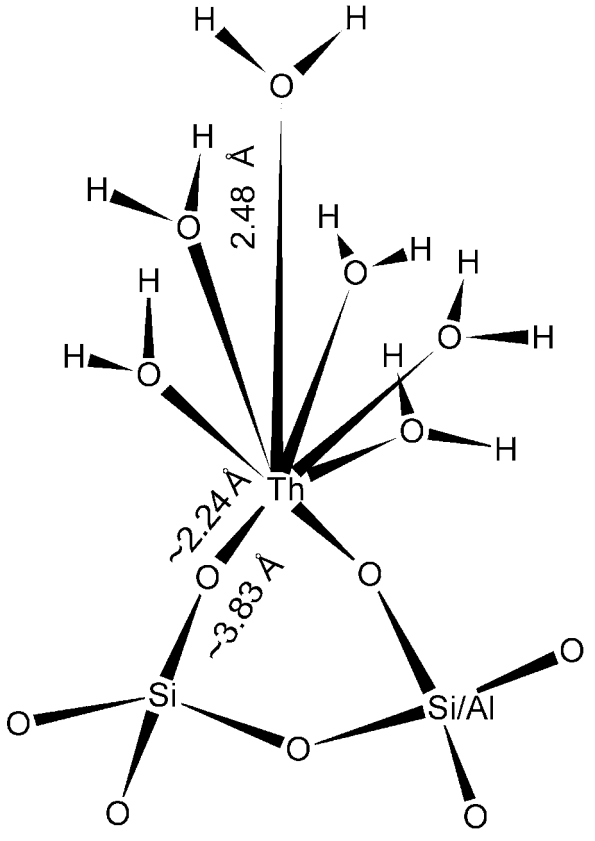

FIG. 10. Schematic structural representation of the Th–Si surface complex. The Th polyhedron is corner-linked to two Si tetrahedra. Distances are not drawn to scale. The number and positions of coordinated water molecules should be seen as rough suggestion only.

4.3. Structure of Th Surface Complexes

The question now to discuss is how Th is bound to the montmorillonite surface. The possibility that Th is incorporated into the montmorillonite structure can rejected because of the considerable size of the Th(IV) ion (1.02 Å) compared to the ionic radii of cations present in the montmorillonite structure (Si(IV) (0.40 Å), Al(III) (0.53 Å), Mg(II) (0.71 Å), and Fe(III) (0.63 Å); (51)). A specific bond of Th atoms to the (001) surface of montmorillonite can be rejected since cation exchanged was prevented due to the high ionic strength (0.1 M $NaClO_4$). Since from the previous discussion the only remaining possibility is that Th is forming a surface complex at the montmorillonite surface, we have illustrated possible Th positions for the montmorillonite structure (Fig. 11) based on the EXAFS bond distances (Table 2). In the following we will discuss some possibilities for a structural link of the Th to the (100), (110), and (010) surfaces of montmorillonite.

Figures 11 and 12 illustrate the montmorillonite structure with models of possible Th surface complexes. In Fig. 11 it was assumed that Th sorbed onto a montmorillonite structure which did undergo congruent dissolution, whereas in Fig. 12 Th sorbed onto a montmorillonite in which the Si tetrahedra were preferentially dissolved (incongruent dissolution; see Section 4.1.3). In neither case could we find positions which are exactly matching 2–3 short Th–O pairs at 2.24 Å and 2–3 Th–Si pairs at 3.83 Å. Nevertheless, we could find possible positions where a Th atom can sorb onto montmorillonite with slightly different distances. Th surface complexes (Th1–Th6, Fig. 11 and Fig. 12) have 2–3 neighboring O atoms at 2.3–2.9 Å and Th–Si/Al pairs at ∼3.9 Å. For example, the complexes Th1 to Th3 shown in

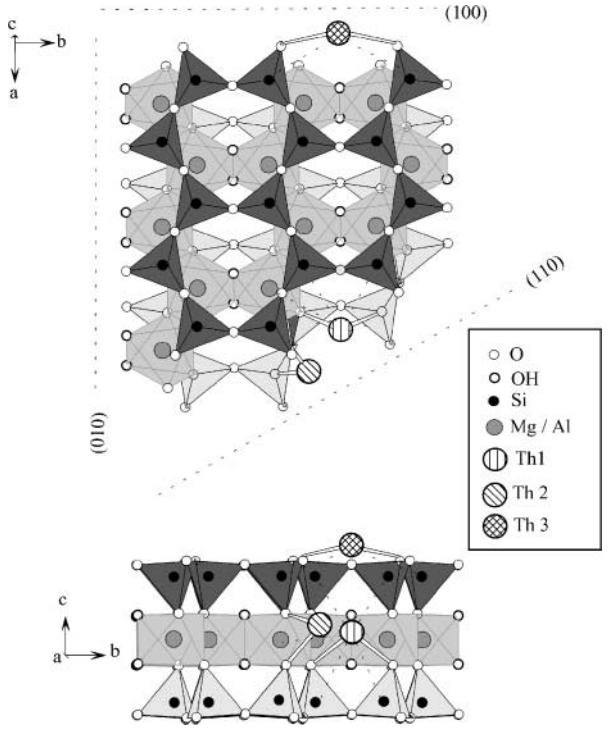

FIG. 11. Idealized particle of montmorillonite bounded by the most common cleavage surfaces, on which three possible Th surface complexes are shown. The nearest Th–O bonds (thick lines) are shown for all three complexes. Nearest Th–Si or Th–Al bonds (broken lines) are shown for complexes Th1 and Th3, but were omitted for Th2 for clarity; structure of montmorillonite is after Tsipursky and Drits (1984).

Fig. 11 possess 2 Si neighboring atoms at 3.8–3.9 Å. Th1 has additionally two Si and one Al neighbor at 3.6 Å. In case that montmorillonite is dissolved incongruently, the illustrated surface complexes (Th4–Th6) possess 1–2 Al neighbors in 3.8–3.9 Å and 2 Al neighbors at 3.5 Å (Th4 and Th5; Fig. 12).

While EXAFS clearly indicated the presence of Th–Si and/or Th–Al pairs at ∼3.9 Å, no backscattering pairs were detected at 3.5–3.6 Å. It is not uncommon in EXAFS data analysis that certain distances cannot be observed. For example, thorite can be fitted reasonably well without taking into account two Th–Si pairs at 3.16 Å, although the presence of this shell is proven by XRD (see Section 3.1, Ref. (40)). The system disorder can cause backscattering pairs to remain undetected. Thus, it is possible that surface complexes such as those illustrated in Figs. 11 and 12 can yield the structural results given in Table 2.

The hypothesis that the system disorder prevents the detection of backscattering pairs is supported by the fact that the spectra at pH 2 and pH 3 (Fig. 4 and Table 2) are almost identical, although the Th surface loading varies by a factor of 40 (for a detailed discussion on surface loading see below). This finding could be understood in the context that there is a wide variety of Th surface complexes which are bound to the montmorillonite surface in different configurations and bond angles.

This hypothesis is supported by the P-EXAFS experiments which were performed on self-supporting clay films treated with Th at pH 2 and 3. The Th P-EXAFS spectra showed no anisotropy in the spectra although the self-supporting clay films were well orientated (Fig. 6; see Section 3.4). Because in P-EXAFS measurements backscattering pairs in the in-plane direction are strongly attenuated when the X-ray polarization vector is parallel to the film plane, there seems to be the lack of a P-EXAFS dependency to indicate that Th is not sorbed to the montmorillonite in the continuity of the octahedral sheet in a single surface complex (see Section 1). A mixture of surface complexes like, e.g., Th1, Th2, Th4, and Th5 which all have bonds to Si that form different angles would severely decrease the P-EXAFS angular dependence (Figs. 11 and 12). It is therefore possible that there is a series of similar complexes in which Th polyhedra bridge to the montmorillonite surface in such a manner that the average angle of the Th–O and Th–Si pairs with respect to the c^* direction (β) is ∼54.7°. At this particular β-angle polarized and powder EXAFS spectra are identical (52) and would eliminate any angular dependence in P-EXAFS measurements.

4.4. Effect of Surface Loading

The results discussed so far suggest that Th is bonded as a surface complex to the montmorillonite surface. To address the question whether the available sorption sites on the

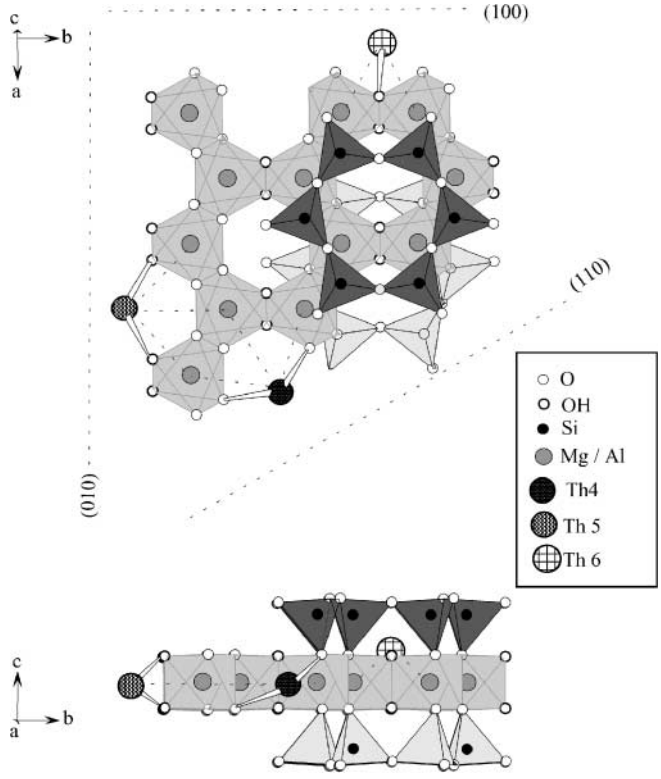

FIG. 12. Simulation of selective dissolution of SiO_4 tetrahedra. This figure is analogous to Fig. 11, but the octahedral sheet is now protruding perpendicular to the (100) and (010) planes due to Si dissolution. Again, three possible Th surface complexes are shown.

montmorillonite surface are saturated, the degree of surface coverage (ratio of the amount sorbed to the amount required to form a monolayer on the particle surface) was estimated.

The number of edge sites can be estimated based on morphological information. Since we lack morphological information on montmorillonite, we used dimensions of hectorite particles (53) to calculate the relative surface area. The relative surface area of montmorillonite edge surfaces (100), (110), and (010) is 2%, assuming that the morphology of montmorillonite and hectorite is similar, although it is not really the case since hectorite particles have an unusual lath shape.

Based on the density of oxygen atoms at the montmorillonite lateral surfaces it is then possible to estimate the number of edge sites (54). This yields 0.5 sites/nm^2 for the lateral surfaces. Because sorption to planar sites was blocked due to the high ionic strength of the solution (0.1 M $NaClO_4$) it is reasonable to assume that mainly edge sites are involved in the uptake process. The estimated number of edge sites (0.5 sites/nm^2) is in the same range as the number of protonable edge sites of montmorillonite deduced by potentiometric titration (1.4 sites/nm^2, (29)). To finally estimate the degree of surface coverage in this study we assumed that Th shares on average 2.5 O atoms with Si tetrahedra from the crystal lattice (Table 2) resulting in 0.2 sites/nm^2 lateral sites. Thus, the edge sites are saturated (surface coverage $>100\%$) when the amount of Th is >32 μmol/g.

Interestingly, the EXAFS spectra and the structural parameters of the low concentrated sample prepared at pH 3 (1–12 μmol/g; surface coverage of 3–38%) are different compared to those of the most concentrated sample (157 μmol/g; surface coverage of 600%). The latter EXAFS spectrum gains certain similarity with the spectrum of an aqueous Th solution (Fig. 7) and CN_{Th-Si} appears to be slightly reduced (2.1 vs 2.7–2.9) compared to samples with a lower surface loading. This finding might indicate that Th is additionally sorbed as an outer-sphere complex when the edge sites are saturated.

5. CONCLUDING REMARKS

The present study investigated for the first time the uptake of Th onto montmorillonite. Two O coordination shells at ~2.24 and ~2.48 Å, and one Si shell at 3.81–3.88 Å, were systematically observed at low and intermediate surface coverage and under reaction conditions either undersaturated or supersatured with respect to amorphous ThO_2. The study showed that at low and intermediate surface coverage the formation of Th nucleation products and Th–Si solution complexes and the sorption of Th on a silica precipitate can be excluded from the EXAFS spectra analysis and solution chemistry and that instead Th is bound to the edges of montmorillonite particles by sharing double corners with Si tetrahedra.

ACKNOWLEDGMENTS

The authors thank the staff of the Rossendorfer Beamline at the ESRF for their support during the EXAFS measurements, and the European Synchrotron Radiation Facility (ESRF) at Grenoble, France, for the provision of beamtime. We acknowledge Juris Purans for fruitful discussions concerning data analysis and Francois Farges for providing the thorite spectrum. Partial financial support was provided by the National Co-operative for the Disposal of Radioactive Waste (Nagra), Wettingen (Switzerland).

REFERENCES

1. Weast, R. C., and Astle, M. J., "CRC Handbook of Chemisty and Physics," Boca Raton, FL, 1983.
2. Santschi, P. H., and Honeymann, B. D., *Radiat. Phys. Chem.* **34,** 213 (1989).
3. Paschoa, A. S., *Appl. Radiat. Isot.* **49,** 189 (1998).
4. Savanonda, N., Prongpunyasakul, E., and Ratanakorn, S., "Quantitative Analysis of Uranium, Thorium and Potassium from Lignite Ash by Neutron Activation Method," Nuclear Data for Basic and Applied Science, Vol. 1, Gordon and Breach, New York, 1985.
5. NAGRA, Nagra Technical Report 93-22, 1994.
6. Güven, N., "Smectites," *in* "Hydrous Phyllosilicates (Exclusive Micas)" (S. W. Bailey, Ed.), Vol. 19, Mineralogical Society of America, 1988.
7. Sposito, G., "The Surface Chemistry of Soils," Oxford University Press, New York, 1984.
8. Stumm, W., and Morgan, J. J., "Aquatic Chemistry, An Introduction Emphasizing Chemical Equilibria in Natural Waters," 2nd ed., Wiley, New York, 1981.
9. Zachara, J. M., Smith, S. C., McKinley, J. P., and Resch, C. T., *Soil Sci. Soc. Am. J.* **57,** 1491 (1993).
10. Zachara, J. M., Smith, S. C., Resch, C. T., and Cowan, C. E., *Soil Sci. Soc. Am. J.* **56,** 1074 (1992).
11. Garcia-Miragaya, J., and Page, A. L., *Soil Sci. Soc. Am. J.* **40,** 658 (1976).
12. Inskeep, W. P., *Soil Sci. Soc. Am. J.* **47,** 660 (1983).
13. Peigneur, P., Maes, A., and Cremers, A., *Clays Clay Miner.* **23,** 71 (1975).
14. McKinley, J. P., Zachara, J. M., Smith, S. C., and Turner, G. D., *Clays Clay Miner.* **43,** 586 (1995).
15. Baeyens, B., and Bradbury, M. H., *J. Contam. Hydrol.* **27,** 199 (1997).
16. Bradbury, M. H., and Baeyens, B., *J. Contam. Hydrol.* **27,** 223 (1997).
17. Bradbury, M. H., and Baeyens, B., *Geochim. Cosmochim. Acta*, in press (2002).
18. Chen, C., and Hayes, K. F., *Geochim. Cosmochim. Acta* **63,** 3205 (1999).
19. Strawn, D. G., and Sparks, D. L., *J. Colloid Interface Sci.* **216,** 257 (1999).
20. Sylwester, E. R., Hudson, E. A., and Allen, P. G., *Geochim. Cosmochim. Acta* **14,** 2431 (2000).
21. Manceau, A., Chateigner, D., and Gates, W. P., *Phys. Chem. Minerals* **25,** 347 (1998).
22. Manceau, A., Schlegel, M. L., Chateigner, D., Lanson, B., Bartoli, C., and Gates, W. P., Application of polarized EXAFS to fine-grained layered minerals, *in* "Synchrotron X-Ray Methods in Clay Science" (D. G. Schulze, J. W. Stucki, and P. M. Bertsch, Eds.), The Clay Mineral Society, 1999.
23. Schlegel, M. L., Manceau, A., Chateigner, D., and Charlet, L., *J. Colloid Interface Sci.* **215,** 140 (1999).
24. Schlegel, M. L., Manceau, A., Charlet, L., Chateigner, D., and Hazemann, J. L., *Geochim. Cosmochim. Acta* **65,** 4155 (2001).
25. Schlegel, M. L., Manceau, A., Charlet, L., and Hazemann, J. L., *Am. J. Sci.*, in press (2002).
26. Dähn, R., Scheidegger, A. M., Manceau, A., Schlegel, M. L., Baeyens, B., and Bradbury, M. H., *J. Synchrotron Rad.* **8,** 533 (2001).
27. Dähn, R., Scheidegger, A. M., Manceau, A., Schlegel, M. L., Baeyens, B., Bradbury, M. H., and Morales, M., *Geochim. Cosmochim. Acta*, in press (2002).
28. Mehra, O. P., and Jackson, M. L., *Clays Clay Miner.* **7,** 317 (1960).
29. Baeyens, B., and Bradbury, M. H., PSI Bericht Nr. 95-10 and Nagra NTB 95-04 (1995).
30. Van Olphen, H., and Fripiat, J. J., "Data Handbook for Clay Materials and Other Non-metallic Minerals," Pergamon Press, New York, 1979.
31. Heydemann, A., *Geochim. Cosmochim. Acta* **30,** 995 (1966).

32. Rai, D., Moore, D. A., Oakes, C. S., and Yiu, M., *Radiochim. Acta* **88,** 297 (2000).
33. Hummel, W., Berner, U., Curti, E., Thoenen, T., and Pearson, J., *Radiochim. acta*, Migration '01 Conference (2001).
34. Baes, C. F., and Mesmer, R. E., "The Hydrolysis of Cations," Wiley, New York, 1976.
35. Ricote, J., and Chateigner, D., *Bol. Soc. Esp. Ceram. Vidrio* **36,** 587 (1999).
36. Bunge, H. J., and Esling, C., "Quantitative Texture Analysis" (H. J. Bunge and C. Esling, Eds.), Deutsche Gesellschaft für Metallkunde, 1982.
37. Matz, W., Schell, N., Bernhard, G., Prokert, F., Reich, T., Claussner, J., Oehme, W., Schlenk, R., Dienel, S., Funke, H., Eichhorn, F., Betzl, M., Prohl, D., Strauch, U., Huttig, G., Krug, H., Neumann, W., Brendler, V., Reichel, P., Denecke, M., and Nitsche, H., *J. Synchrotron Rad.* **6,** 1076 (1999).
38. Ressler, T., *J. Synchrotron Rad.* **5,** 118 (1998).
39. Rehr, J. J., Mustre de Leon, J., Zabinsky, S., and Albers, R. C., *J. Am. Chem. Soc.* **113,** 5135 (1991).
40. Taylor, M., and Ewing, R. C., *Acta Crystallogr. Sect. B* **34,** 1074 (1978).
41. Moll, H., Denecke, M. A., Jalilehvand, J., Sandström, M., and Grenthe, I., *Inorg. Chem.* **38,** 1795 (1999).
42. Wyckoff, R. W. G., "Crystal Structure," 2nd ed., Vol. 1, Wiley, New York, 1963.
43. Östhols, E., Manceau, A., Farges, F., and Charlet, L., *J. Colloid Interface Sci.* **194,** 10 (1997).
44. Farges, F., *Geochim. Cosmochim. Acta* **55,** 3303 (1991).
45. Crozier, E. D., Rehr, J. J., and Ingalls, I., *in* "X-Ray Absorption: Principles Applications, Techniques of EXAFS, SEXAFS and XANES," Wiley, New York, 1988.
46. Bunker, G., *Nucl. Instrum. Meth. Phys. Res.* **207,** 437 (1983).
47. Stern, E. A., *Phys. Rev. B Condens. Matter* **48,** 9825 (1993).
48. Johansson, G., Magini, M., and Ohtaki, H. *J. Solution Chem.* **20,** 775 (1991).
49. White, A. F., Chemical weathering rates of silicate minerals in soils, *in* "Chemical Weathering Rates of Silicate Minerals" (A. F. White and S. L. Brantley, Eds.), Mineralogical Society of America, Washington DC, 1996.
50. Rimstidt, J. D., and Barnes, H. L., *Geochim. Cosmochim. Acta* **44,** 1683 (1980).
51. Shannon, R. D., *Acta Crystallogr. Sect. A* **32,** (1976).
52. Manceau, A., Bonnin, D., Stone, W. E. E., and Sanz, J., *Phys. Chem. Miner.* **17,** 363 (1990).
53. Schlegel, M. L., Manceau, A., and Charlet, L., *J. Colloid Interface Sci.* **220,** 392 (1999).
54. Tsipursky, S. I., and Drits, V. A., *Clay Miner.* **19,** 177 (1984).